Kink distortion of the pseudo-S_4 axis in pseudotetrahedral [N_2O_2] bis-chelate cobalt(II) single-ion magnets leads to increased magnetic anisotropy

Sudhir Lima,[a,b] Maximilian H. Pohle,[a] Michael Böhme,[a] Helmar Görls,[a] Thomas Lohmiller,[c,d] Alexander Schnegg,[d,e] Rupam Dinda,*[b] and Winfried Plass*[a]

[a] Institut für Anorganische und Analytische Chemie, Friedrich-Schiller-Universität Jena, Humboldtstr. 8, 07743 Jena, Germany.

[b] Department of Chemistry, National Institute of Technology, Rourkela, 769008 Odisha, India.

[c] Humboldt-Universität zu Berlin, Institut für Chemie, Brook-Taylor-Str. 2, 12489 Berlin, Germany.

[d] EPR4 Energy Joint Lab, Department Spins in Energy Conversion and Quantum Information Science, Helmholtz Zentrum Berlin für Materialien und Energie GmbH, Albert-Einstein-Straße 15, 12489 Berlin, Germany.

[d] *EPR Research Group, Max Planck Institute for Chemical Energy Conversion, Stiftstrasse 34-36, 45470 Mülheim an der Ruhr, Germany*.

Electronic Supplementary Information (ESI)

Table S1 Crystal data and refinement parameters for **1** and **2**

	1	**2**
empirical formula	$C_{36}H_{36}CoN_6O_2S_2$	$C_{38}H_{40}CoN_6O_2S_2$
formula weight / g mol^{-1}	707.76	735.81
crystal size / mm^3	0.102 x 0.088 x 0.082	0.102 x 0.094 x 0.078
crystal system	monoclinic	monoclinic
space group	$P2_1/c$ (no. 14)	$C\,2/c$ (no. 15)
a / pm	1323.78(6)	1932.24(3)
b / pm	1140.15(5)	1496.33(4)
c / pm	2139.70(9)	1321.76(3)
α / deg	90	90
β / deg	92.190(2)	101.407(1)
γ / deg	90	90
V / 10^6 pm^3	3227.1(2)	3746.08(14)
T / K	133(2)	133(2)
δ_{calc} / g cm^{-3}	1.457	1.305
Z	4	4
λ / pm	71.073	71.073
F(000)	1476	1540
μ(Mo K$_\alpha$) / mm^{-1}	0.706	0.611
Θ range for data collection / deg	$1.539 \leq \Theta \leq 27.475$	$2.150 \leq \Theta \leq 27.485$
ranges of reflection indices	$-12 \leq h \leq 17$	$-25 \leq h \leq 25$
	$-14 \leq k \leq 14$	$-19 \leq k \leq 19$
	$-27 \leq l \leq 27$	$-17 \leq l \leq 17$
measured reflections	28598	24526
independent reflections	7367	3830
reflections used	7367	3830
R_{int}	0.0614	0.0404
no. of parameters	428	293
no. of restraints	0	269
completeness to Θ = 25.242°	0.999	0.999
refinement method	full-matrix least-squares on F^2	full-matrix least-squares on F^2
goodness-of-fit on F^2	1.114	1.125
R_1 (all data)	0.1036	0.0586
R_1 ($I > 2\sigma[I]$)	0.0712	0.0513
wR_2 (all data)	0.1417	0.1238
wR_2 ($I > 2\sigma[I]$)	0.1296	0.1197
$\Delta\rho_{max}$ ($\Delta\rho_{min}$) / e Å^{-3}	0.475 (−0.556)	1.414 (−0.551)
CCDC deposition number	CCDC-2247543	CCDC-2247544

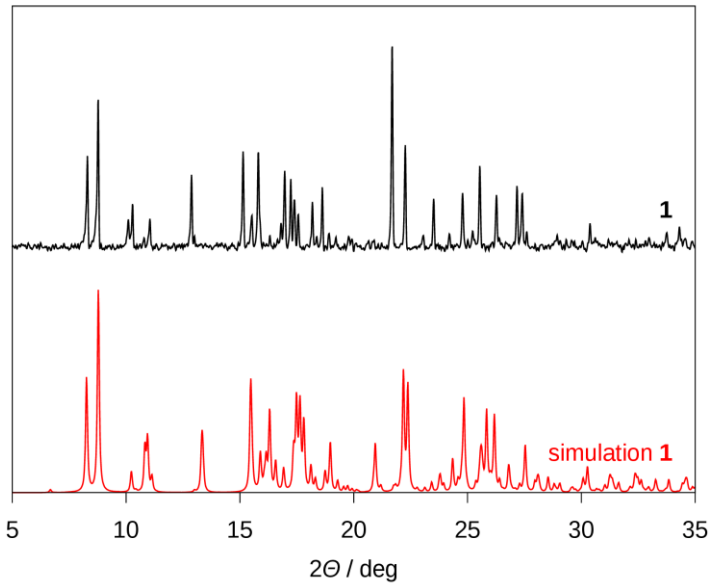

Fig. S1 Powder X-ray diffraction (PXRD) pattern of **1** (black: experiment at room temperature; red: simulation based on the crystal structure measured at 133 K).

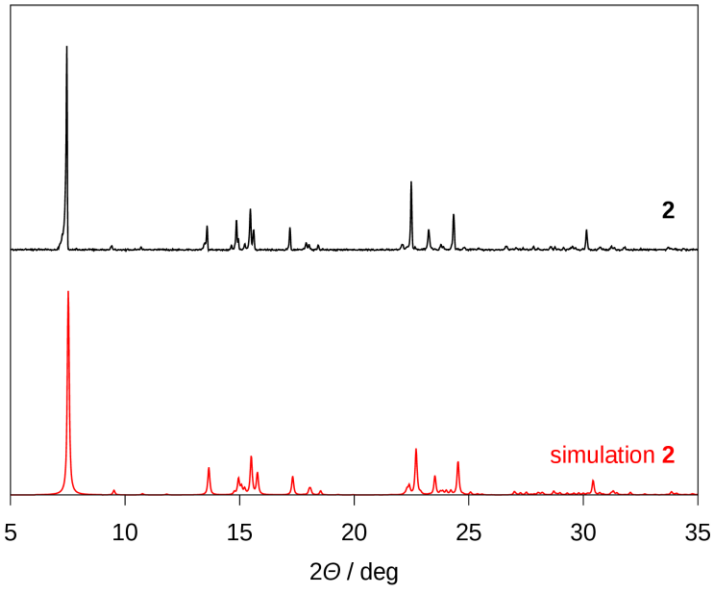

Fig. S2 Powder X-ray diffraction (PXRD) pattern of **2** (black: experiment at room temperature; red: simulation based on the crystal structure measured at 133 K).

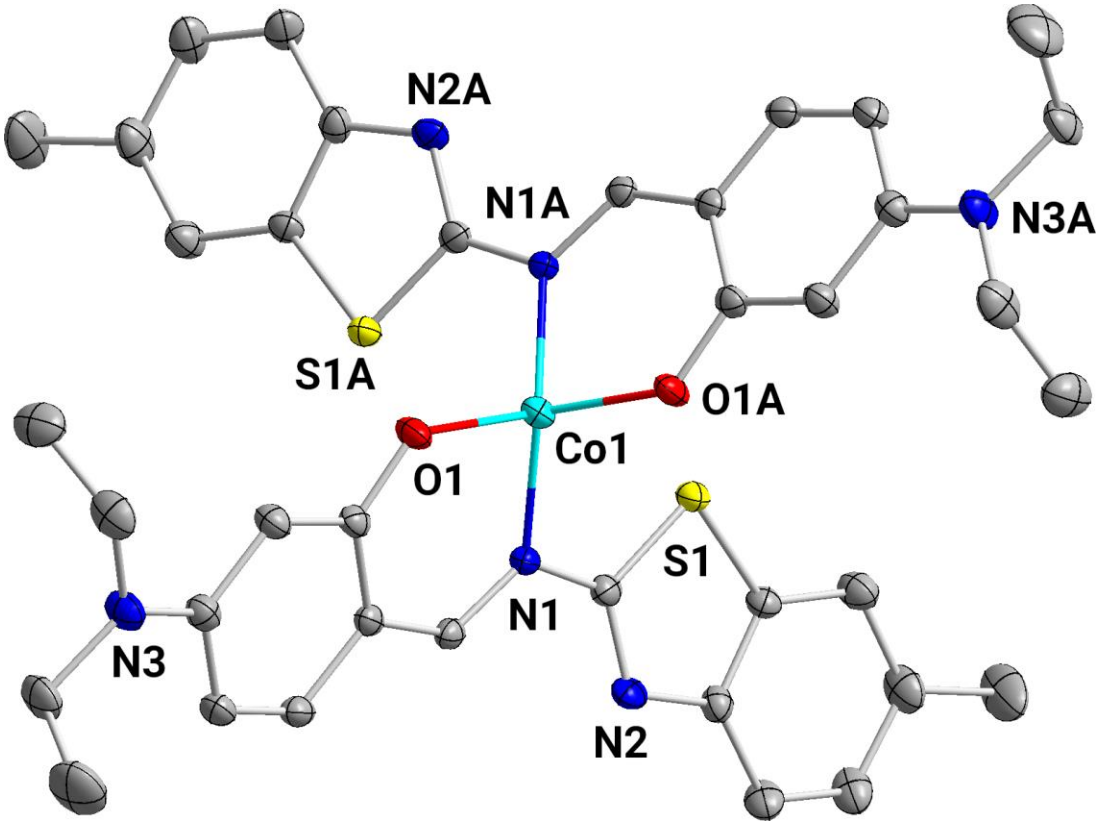

Fig. S3 Molecular structure of the minor component of **2** with the disordered position of the benzothiazole moiety (occupancy 0.1). Color code: Co (cyan), N (blue), O (red), and S (yellow). Thermal ellipsoids are drawn at the 50% probability level. Hydrogen atoms are omitted for clarity.

Table S2 Comparison of structural parameters for homoleptic pseudotetrahedral cobalt(II) bis-chelate complexes with $[N_2O_2]$ donor set together with the determined spin-reversal barrier U_{Orb} (**3**: $[Co(L^{Sal,2\text{-}Ph})_2]$; $HL^{Sal,2\text{-}Ph}$: 2-(([1,1'-biphenyl]-2-ylimino)methyl)phenol; **4**: $[Co(L^{Nph,2\text{-}Ph})_2]$; $HL^{Nph,2\text{-}Ph}$: 1-[*N*-(2-phenylphenyl)carboximidoyl]naphthalen-2-ol; **5**: $[Co(L^{Nph,4\text{-}Br})_2]$; $HL^{Nph,4\text{-}Br}$: 1-[*N*-(4-bromophenyl)carboximidoyl]naphthalen-2-ol)

Entry	α_o[a] / deg	α_a[b] / deg	κ / deg	$(180 - \kappa)$ / deg	δ / deg	$(90 - \delta)$ / deg	ε_T	U_{Orb}[c] / cm^{-1}	Ref.
1	116.6	94.9	163.2	16.8	88.9	1.1	1.23	58.9	this work
2	116.9	94.8	167.4	12.6	87.5	2.5	1.23	60.5[d]	this work
3·$2CH_3OH$	119.2	94.6	178.1	1.9	55.9	34.1	1.26	55.3	[13]
3	117.8	94.8	174.4	5.6	72.5	17.5	1.24	47.3	[12, 13]
4	119.3	93.0	177.8	2.2	65.3	24.7	1.28	62.8	[12, 13]
4·CH_2Cl_2	117.9	93.5	173.1	6.9	78.8	11.2	1.26	50.6	[8, 13]
5	116.6	94.4	174.0	6.0	85.6	4.4	1.24	52.4[e]	[8]

[a] Average obtuse bond angle α_o determined from the four bond angles not given by the chelate ligands. [b] Average acute bond angle α_a given by the two bite angles of the chelate ligands. [c] Determined by FD-FT THz-EPR if not stated otherwise. [d] Determined by simultaneous fitting of susceptibility and magnetization data. [e] Determined by fitting of susceptibility data and assuming $U_{Orb} = |2D|$.

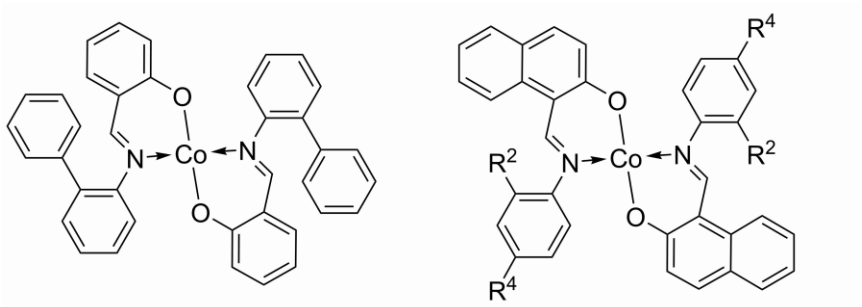

$[Co(L^{Sal,2\text{-}Ph})_2]$ (**3**)

$[Co(L^{Nph,2\text{-}Ph})_2]$ (**4**) R^2 = Ph, R^4 = H

$[Co(L^{Nph,4\text{-}Br})_2]$ (**5**) R^2 = H, R^4 = Br

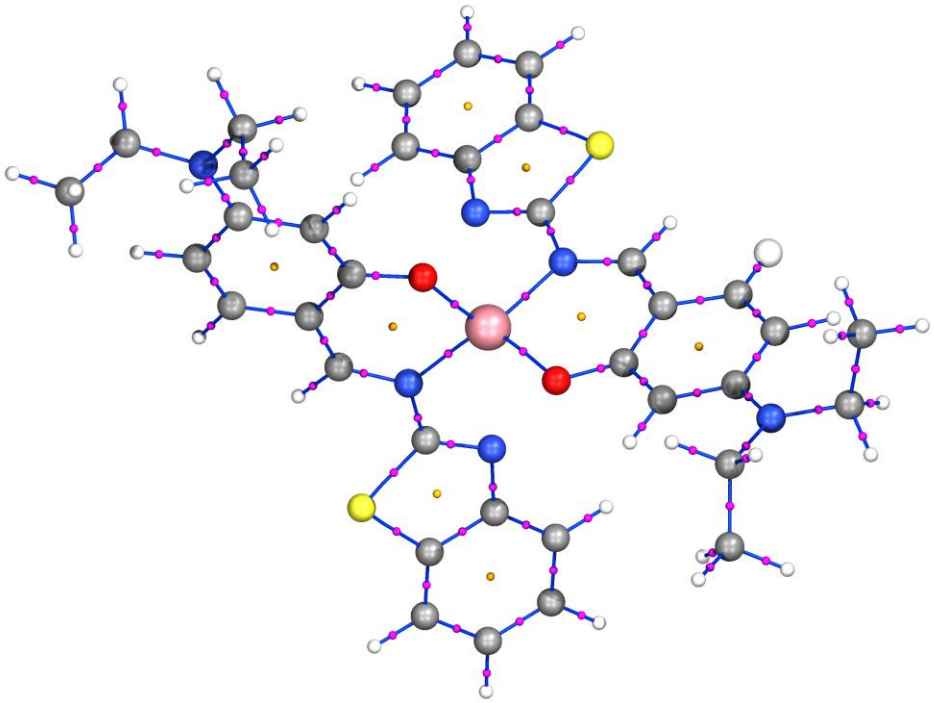

Fig. S4 QTAIM distribution of critical points (color code: pink – bond critical points; orange – ring critical points) and bond paths (blue lines) for **1** as obtained from DFT/TPSSh/def2-TZVPP level of theory.

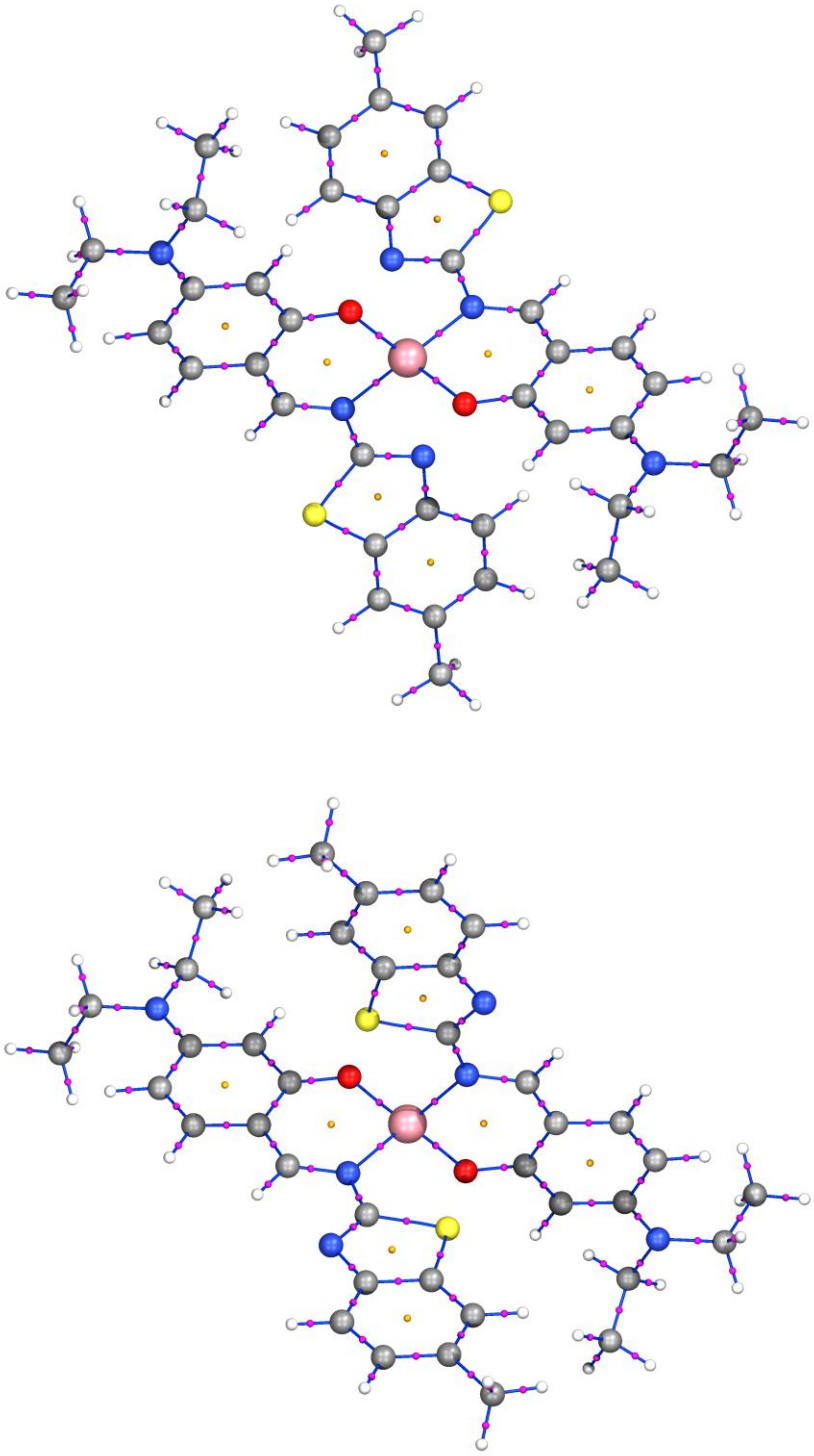

Fig. S5 QTAIM distribution of critical points (color code: pink – bond critical points; orange – ring critical points) and bond paths (blue lines) for the major component with an occupancy of 0.9 (top) and the minor component with a factor of 0.1 (bottom) of **2** as obtained from calculations on the DFT/TPSSh/def2-TZVPP level of theory.

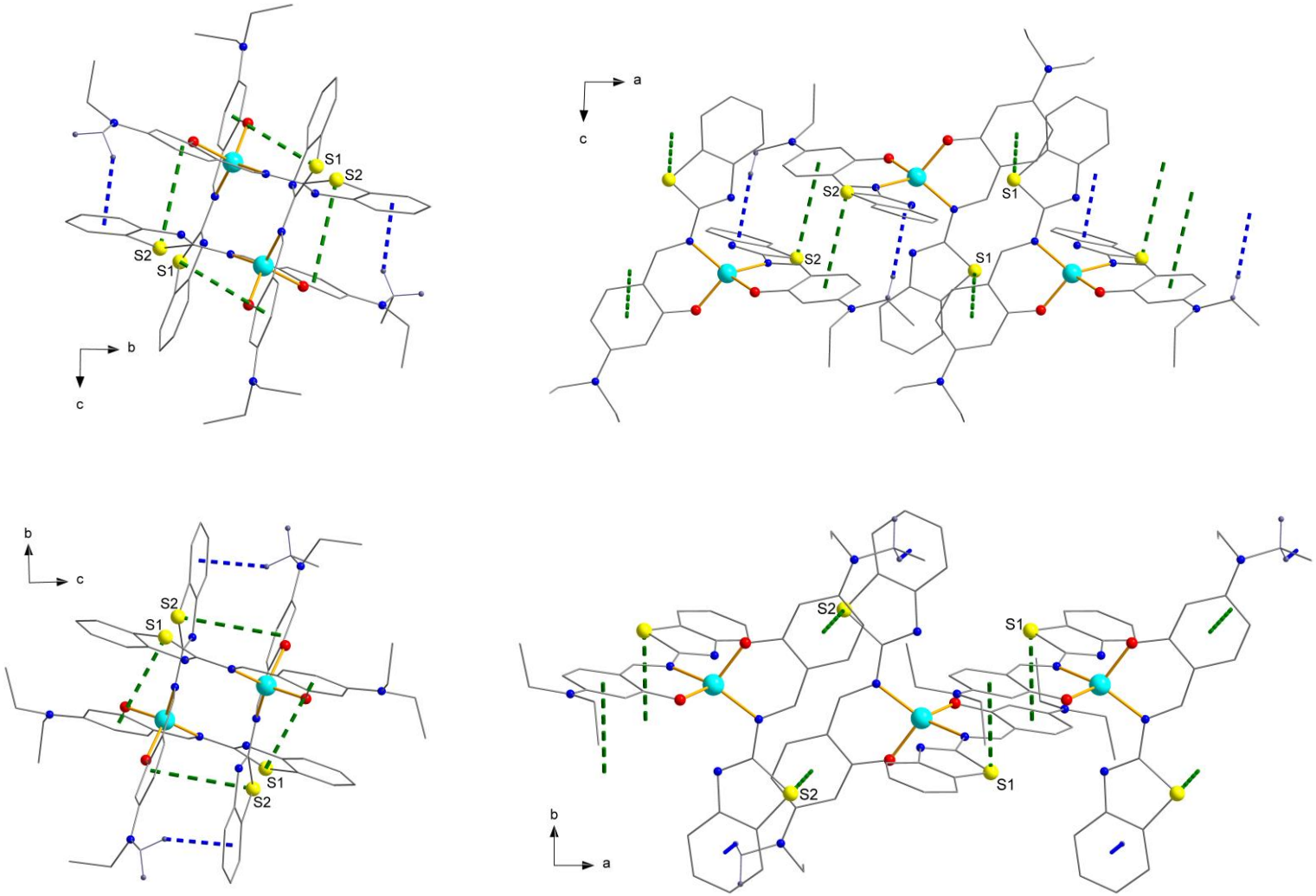

Fig. S6 Representation of the packing for complex **1** showing the formation of chains with π interactions. View along the [100] direction (left column) and side views along the [010] (top right) and the [001] direction (bottom right). Color code: Co – cyan, S – yellow, O – red, N – blue. The green dashed lines represent intermolecular lp(S)/π···π interactions (S1···centroid 353 pm; S2···centroid 385 pm) and the blue dashed lines C–H···π interactions (H···centroid 249 pm, C–H···centroid 150°). Closest intermolecular Co···Co distance along the chain in crystallographic *a* direction is found at 711 pm. Hydrogen atoms except those of the CH_2 groups involved in C–H···π interactions have been omitted for clarity.

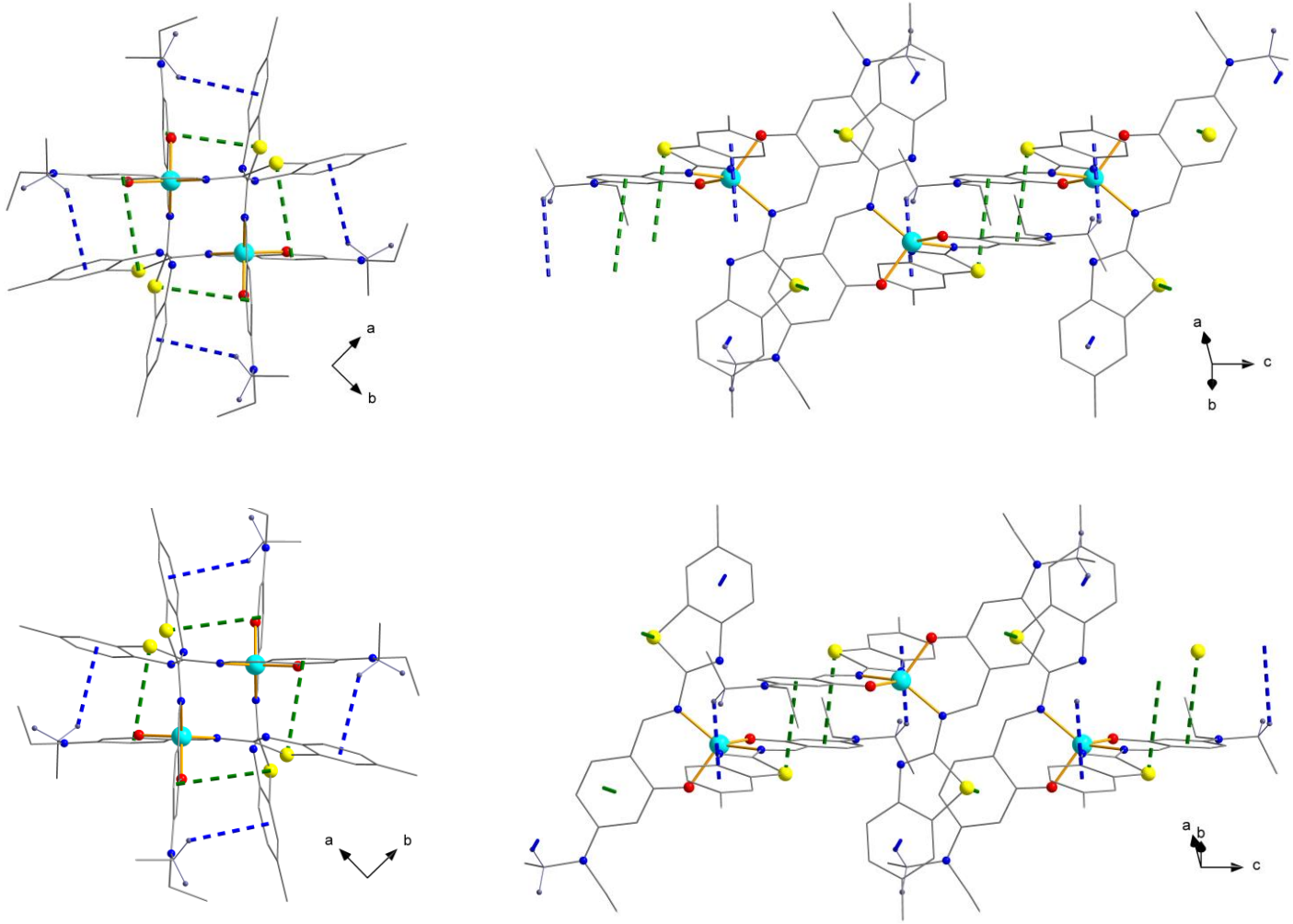

Fig. S7 Representation of the packing for complex **2** showing the formation of chains with π interactions. View along the [001] direction (left column) and side views along the [-1-10] (top right) and [1-10] direction (bottom right). Color code: Co – cyan, S – yellow, O – red, N – blue. The green dashed lines represent intermolecular lp(S)/π···π interactions (S···centroid 351 pm) and the blue dashed lines C–H···π interactions (H···centroid 299 pm, C–H···centroid 133°). Closest intermolecular Co···Co distance along the chain in crystallographic *a* direction is found at 760 pm. Hydrogen atoms except those of the CH_2 groups involved in C–H···π interactions have been omitted for clarity.

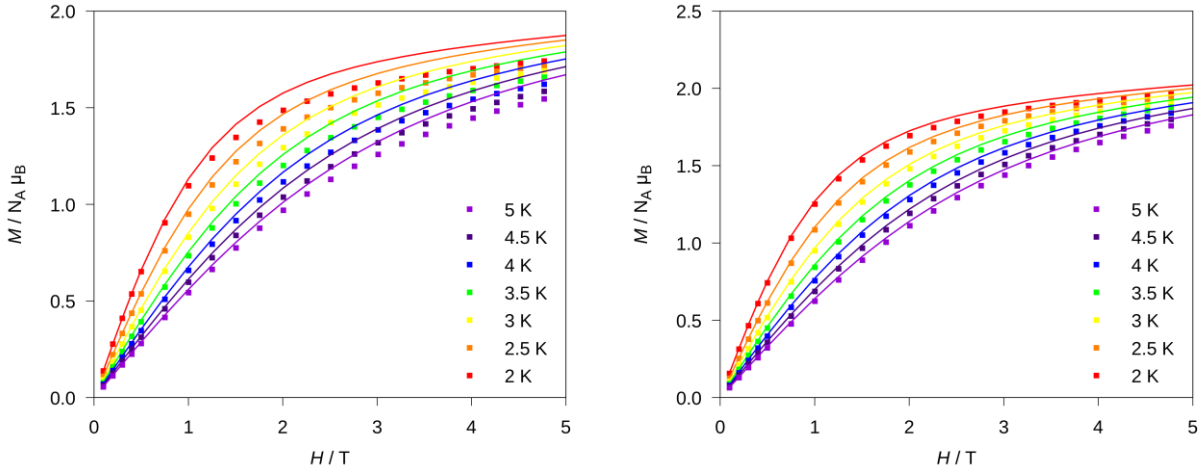

Fig. S8 Magnetization data up to 5 T at different temperatures between 2 and 5 K for complex **1** (left) and **2** (right). Lines represent the simulation according to eqn (1) using the parameters given in the text.

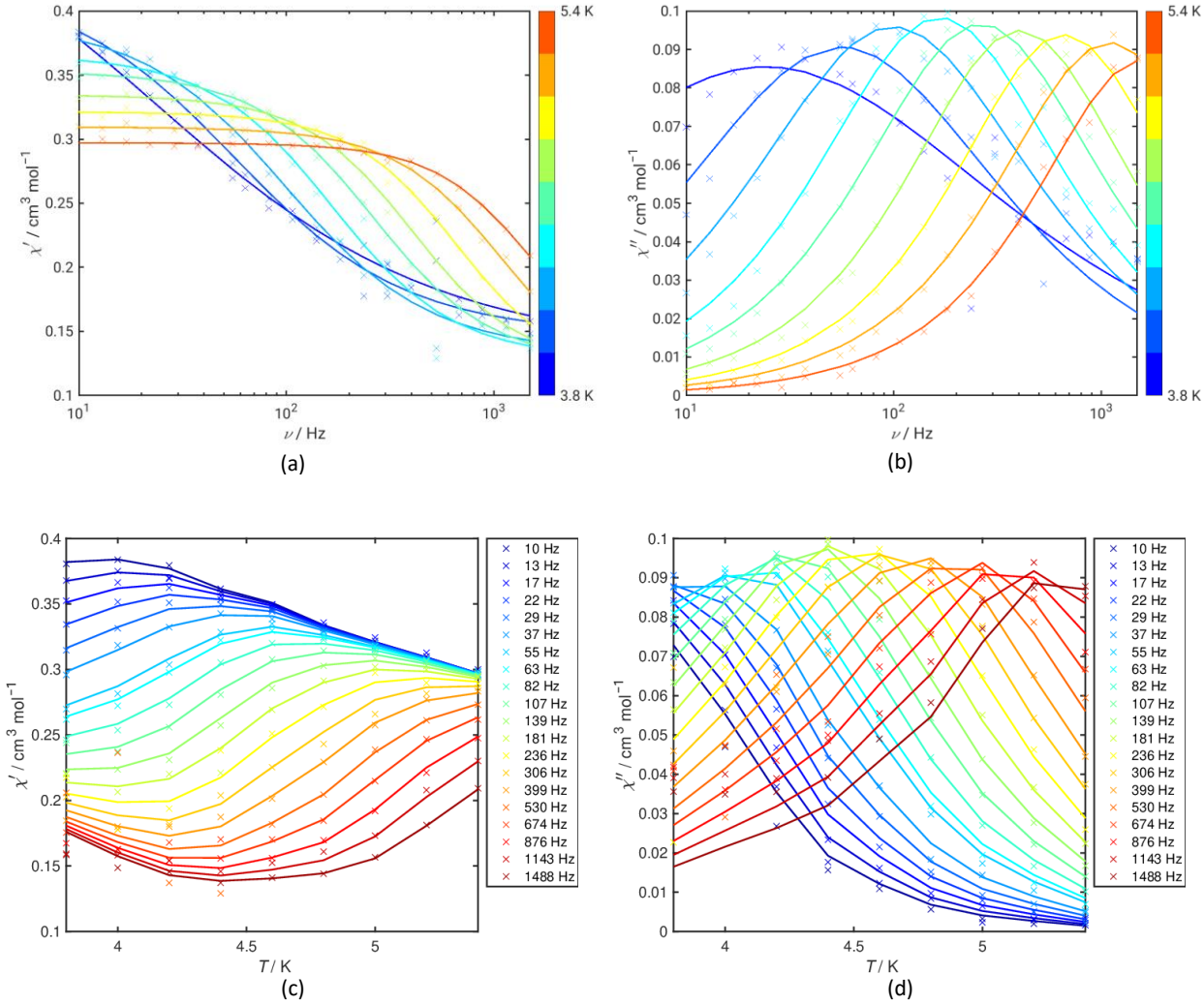

Fig. S9 Frequency (top) and temperature (bottom) dependence of the in-phase (left) and out-of-phase (right) ac susceptibility data for **1** with a static field of 40 mT. Lines represent fitted values according to eqn (2) from the main manuscript.

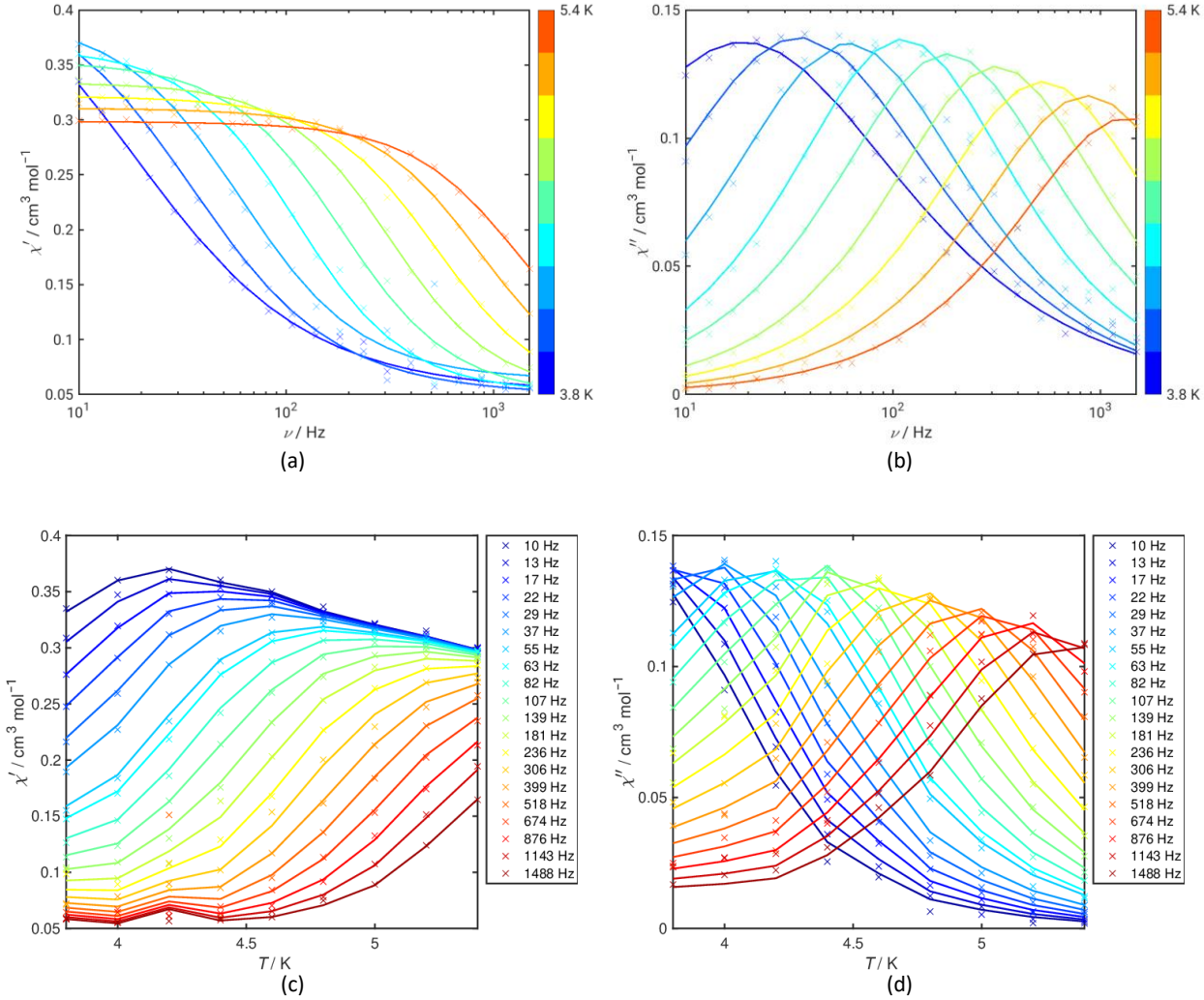

Fig. S10 Frequency (top) and temperature (bottom) dependence of the in-phase (left) and out-of-phase (right) ac susceptibility data for **1** with a static field of 100 mT. Lines represent fitted values according to eqn (2) from the main manuscript.

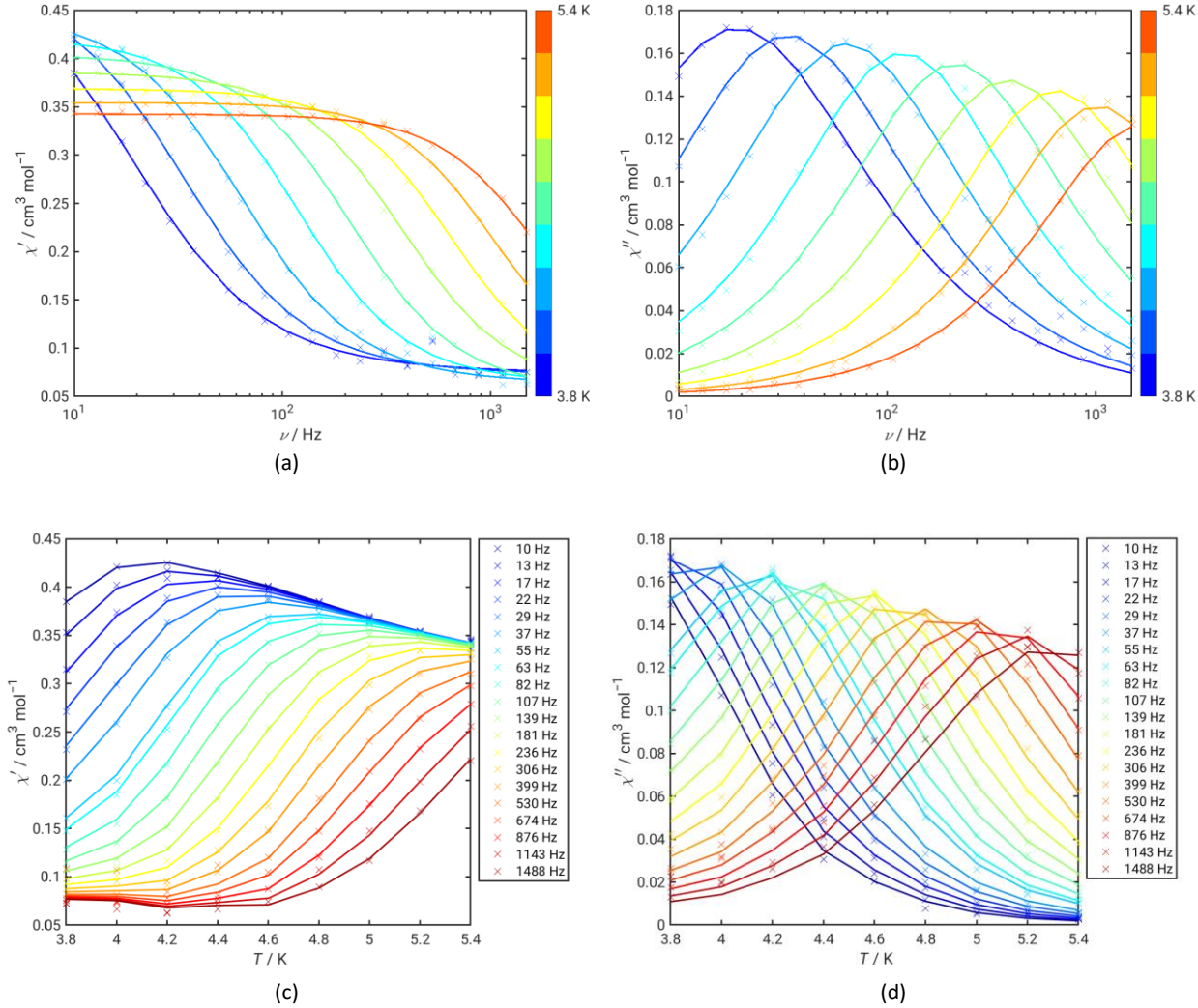

Fig. S11 Frequency (top) and temperature (bottom) dependence of the in-phase (left) and out-of-phase (right) ac susceptibility data for **2** with a static field of 40 mT. Lines represent fitted values according to eqn (2) from the main manuscript.

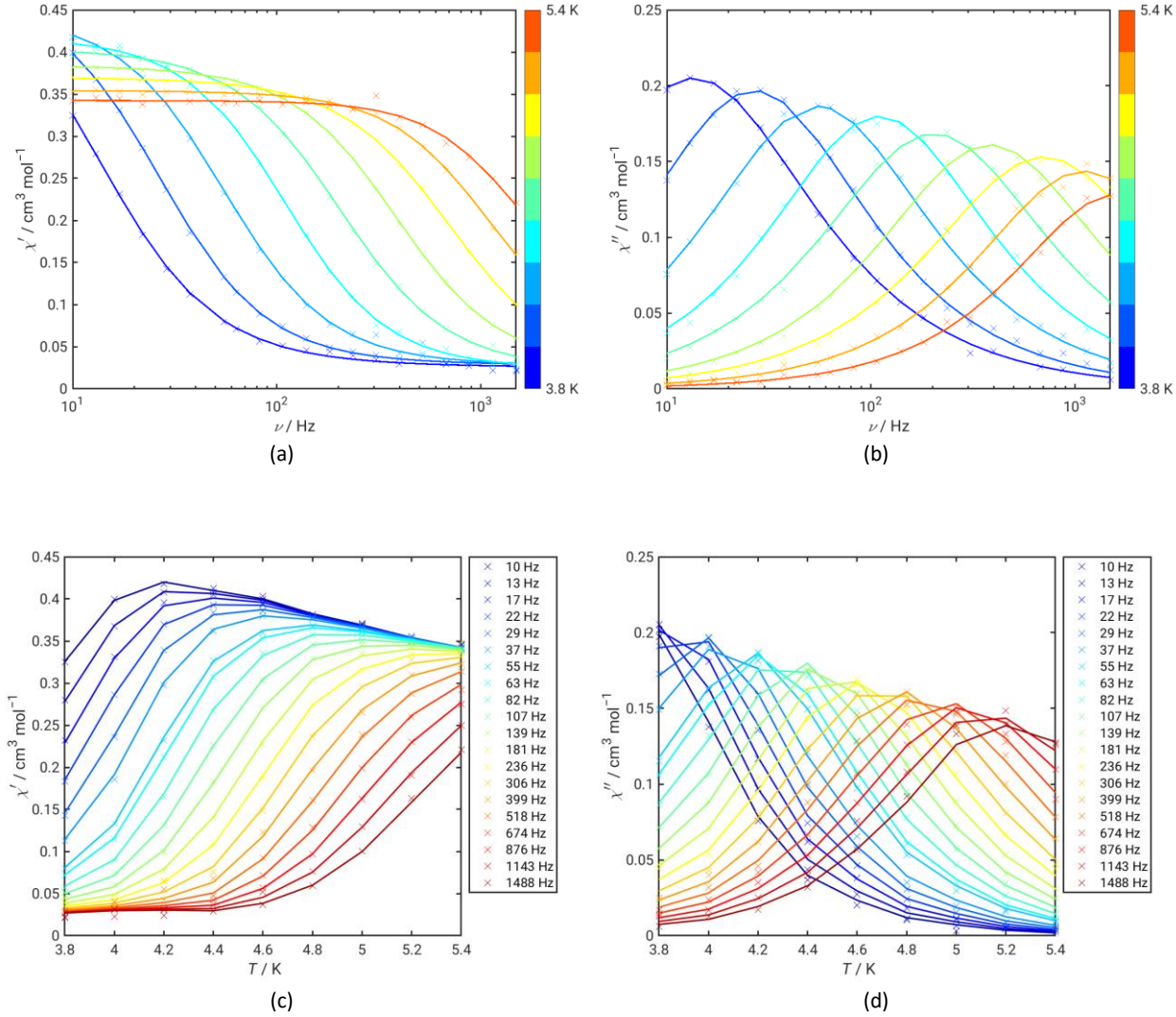

Fig. S12 Frequency (top) and temperature (bottom) dependence of the in-phase (left) and out-of-phase (right) ac susceptibility data for **2** with a static field of 100 mT. Lines represent fitted values according to eqn (2) from the main manuscript.

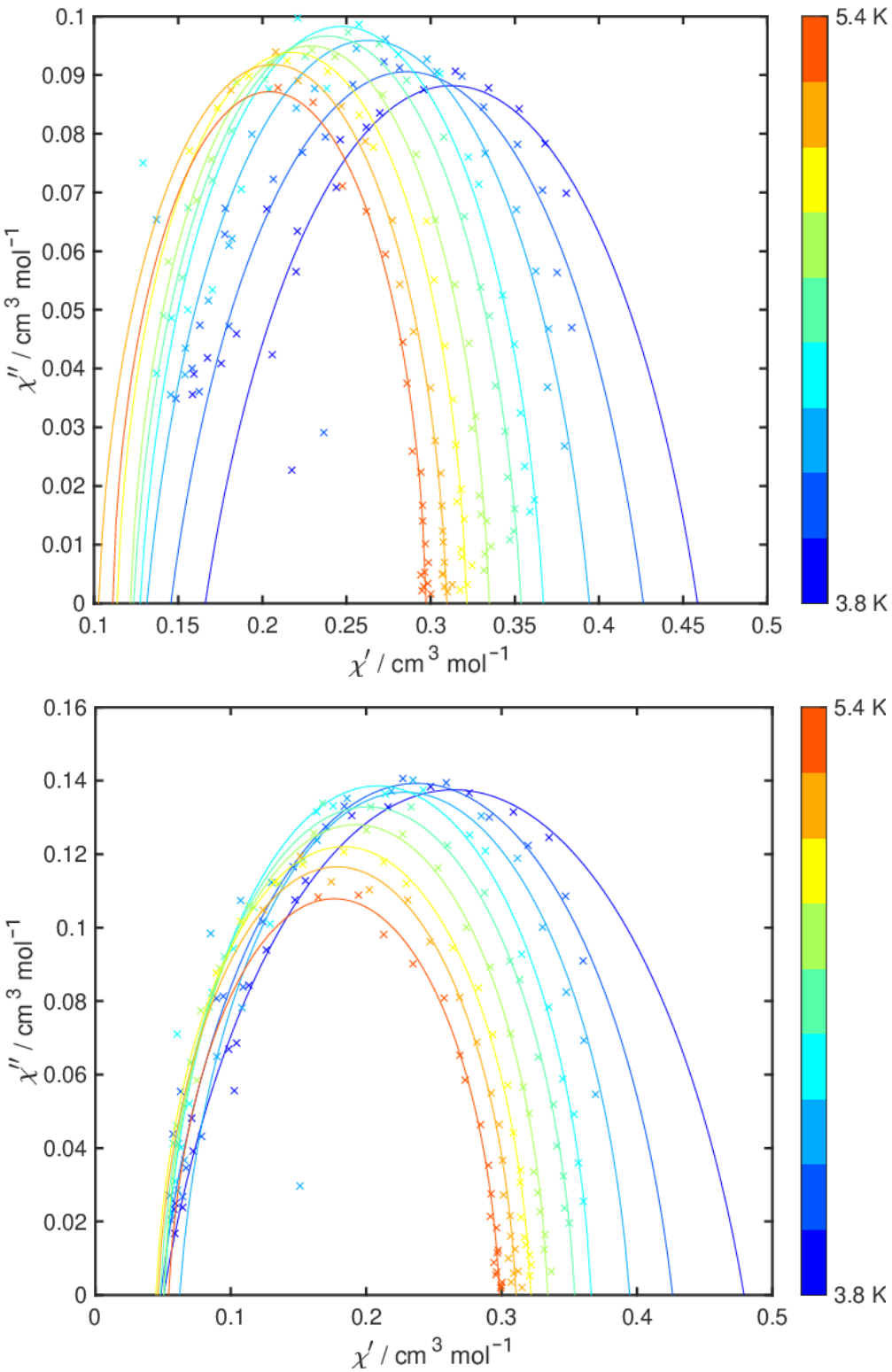

Fig. S13 Cole–Cole plot for **1** at static fields of 40 mT (top) and 100 mT (bottom). Lines represent fitted values according to eqn (2) from the main manuscript.

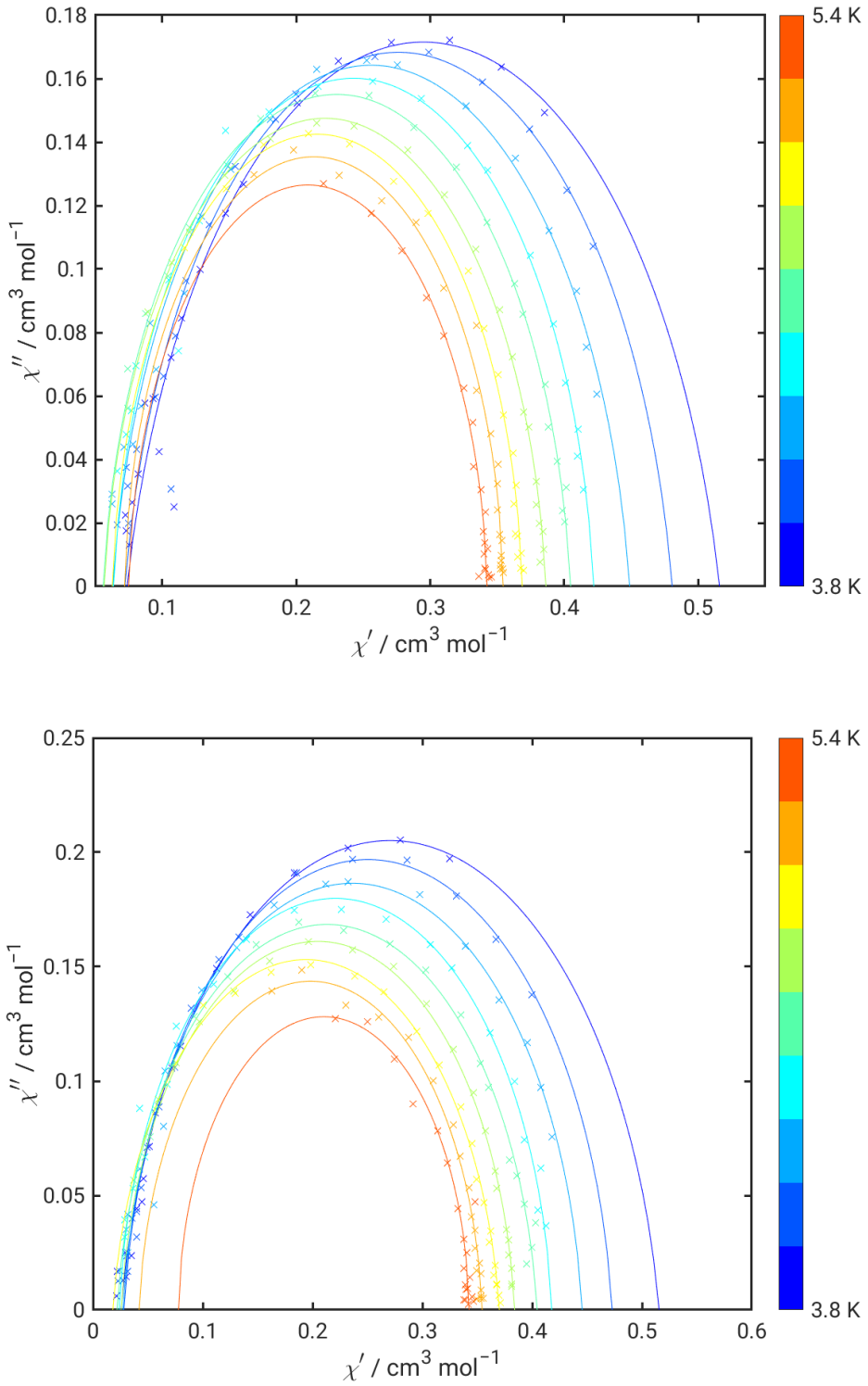

Fig. S14 Cole–Cole plot for **2** at static fields of 40 mT (top) and 100 mT (bottom). Lines represent fitted values according to eqn (2) from the main manuscript.

Table S3 Temperature-dependent relaxation times τ_c and fitting parameters α, χ_S, and χ_0 for the Cole–Cole plots of **1** at 40 mT

T / K	χ_S / emu mol^{-1}	χ_0 / emu mol^{-1}	τ_c / 10^{-3} s	α
3.8	0.1660	0.4586	5.2345	0.3091
4.0	0.1455	0.4263	2.8445	0.2705
4.2	0.1313	0.3943	1.6050	0.1974
4.4	0.1273	0.3670	0.9554	0.1253
4.6	0.1234	0.3537	0.6052	0.1110
4.8	0.1216	0.3348	0.3938	0.0734
5.0	0.1137	0.3215	0.2412	0.0646
5.2	0.1027	0.3096	0.1450	0.0762
5.4	0.1110	0.2972	0.1015	0.0417

Table S4 Temperature dependent relaxation times τ_c and fitting parameters α, χ_S, and χ_0 for the Cole–Cole plots of **1** at 100 mT

T / K	χ_S / emu mol^{-1}	χ_0 / emu mol^{-1}	τ_c / 10^{-3}s	α
3.8	0.0503	0.4791	8.4118	0.2738
4.0	0.0483	0.4263	4.4978	0.1914
4.2	0.0622	0.3945	2.6271	0.1227
4.4	0.0507	0.3662	1.4324	0.0821
4.6	0.0478	0.3540	0.8698	0.0897
4.8	0.0504	0.3341	0.5058	0.0652
5.0	0.0447	0.3217	0.3020	0.0805
5.2	0.0462	0.3107	0.1848	0.0802
5.4	0.0541	0.2986	0.1197	0.0796

Table S5 Temperature dependent relaxation times τ_c and fitting parameters α, χ_S, and χ_0 for the Cole–Cole plots of **2** at 40 mT

T / K	χ_S / emu mol^{-1}	χ_0 / emu mol^{-1}	τ_c / 10^{-3}s	α
3.8	0.0737	0.5159	8.3404	0.1598
4.0	0.0721	0.4806	4.7337	0.1224
4.2	0.0629	0.4488	2.4975	0.1020
4.4	0.0636	0.4220	1.3410	0.0715
4.6	0.0559	0.4047	0.7517	0.0747
4.8	0.0566	0.3863	0.4193	0.0704
5.0	0.0627	0.3687	0.2487	0.0452
5.2	0.0719	0.3544	0.1552	0.0269
5.4	0.0748	0.3424	0.0958	0.0357

Table S6 Temperature dependent relaxation times τ_c and fitting parameters α, χ_S, and χ_0 for the Cole–Cole plots of **2** at 100 mT

T / K	χ_S / emu mol^{-1}	χ_0 / emu mol^{-1}	τ_c / 10^{-3}s	α
3.8	0.0254	0.5155	11.7441	0.1125
4.0	0.0281	0.4728	5.9422	0.0773
4.2	0.0272	0.4455	2.9005	0.0728
4.4	0.0238	0.4178	1.4475	0.0577
4.6	0.0218	0.4045	0.7813	0.0808
4.8	0.0256	0.3840	0.4167	0.0677
5.0	0.0181	0.3701	0.2267	0.0883
5.2	0.0420	0.3544	0.1437	0.0532
5.4	0.0779	0.3424	0.1006	0.0202

Table S7 Relative CASSCF and CASPT2 energies (in cm^{-1}) for all quartet and the 12 lowest doublet states of **1**, **2**, **2** (κ = 170°), and **2** (κ = 160°)

2*S*+1	Term	Subterm	**1**		**2**		**2** (κ = 170°)		**2** (κ = 160°)	
			CASSCF	CASPT2	CASSCF	CASPT2	CASSCF	CASPT2	CASSCF	CASPT2
4	^4F	$^4A_2$	0	0	0	0	0	0	0	0
		$^4T_2$	1924	2007	2119	2046	2169	2102	1905	1810
			6003	6435	6155	6613	6258	6751	5645	5955
			6418	6868	6876	7608	6875	7611	6898	7342
		$^4T_1$	7422	7878	8213	8158	8299	8121	7525	7627
			7772	8334	8237	8396	8359	8290	7972	7782
			9346	9514	9187	8840	9052	8440	9902	10092
	^4P	$^4T_1$	21598	19137	21660	19089	21589	18832	21748	18967
			22915	20094	23346	20459	23421	20299	23075	19937
			23330	20668	23720	21187	23870	21201	23266	20315
2	$^2G + {}^2P$		18322	15445	18379	15247	18444	15214	17861	15037
			18374	15528	18746	15439	18825	15437	18374	15244
			19803	16866	19927	16695	19922	16665	19953	16696
			20060	17162	20143	17088	20127	17047	20238	17126
			20398	17573	20576	17406	20594	17414	20429	17257
			20661	17848	20785	17695	20815	17699	20664	17379
			21651	18873	21850	18953	21905	18985	21657	18750
			23742	21003	24181	21134	24329	21072	23563	20766
			24691	22458	24969	21962	24874	21965	24987	21542
			25061	22207	25093	22048	25111	21965	25163	21899
			25256	21767	25541	22218	25585	22197	25410	22002
			25627	22055	25929	22566	25993	22543	25728	22533
	…	…	…	…	…	…	…	…	…	…

Table S8 Relative SO-RASSI energies (in cm^{-1}) for the lowest Kramers doublets (KDs) of **1**, **2**, **2** (κ = 170°), and **2** (κ = 160°)

Term		KD	**1**	**2**	**2** (κ = 170°)	**2** (κ = 160°)
^4F	$^4A_2$	1	0	0	0	0
		2	64	66	64	74
	$^4T_2$	3	2095	2123	2176	1887
		4	2240	2266	2319	2040
		5	6104	6485	6636	5829
		6	6348	6671	6786	5973
		7	6876	7513	7368	7313
		8	6994	7594	7532	7448
	$^4T_1$	9	7965	8021	7801	7666
		10	8129	8318	8168	7870
		11	8540	8495	8326	8104
		12	8718	8914	8600	8219
		13	9667	9028	9009	10128
		14	9778	9251	9134	10159

Table S9 Calculated zero-field splitting (ZFS) parameters and their Cartesian components of the g-tensor for S_{eff} = 3/2 of the $^4A_2[^4F]$ ground multiplet of complexes **1**, **2**, **2** (κ = 170°), and **2** (κ = 160°) with $g_{av} = \sqrt{(g_x^2 + g_y^2 + g_z^2)/3}$

	D / cm^{-1}	E / cm^{-1}	$\lvert E/D \rvert$	g_{av}	g_x	g_y	g_z
1	−31.9	−0.9	0.03	2.302	2.150	2.165	2.566
2	−33.0	−0.7	0.02	2.297	2.138	2.159	2.568
2 (κ = 170°)	−32.2	−0.4	0.01	2.284	2.140	2.156	2.557
2 (κ = 160°)	−36.9	−1.4	0.04	2.306	2.133	2.166	2.617

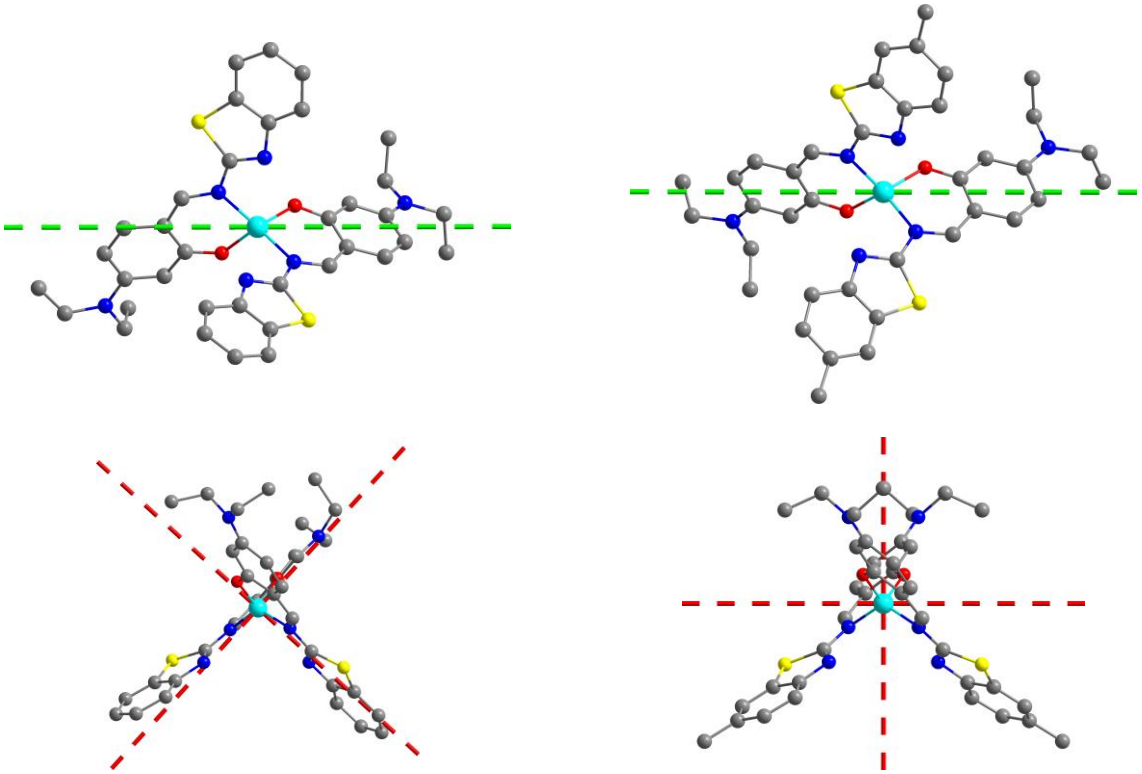

Fig. S15: *Ab initio* calculated anisotropy axes of the $^4A_2[^4F]$ ground multiplet for S_{eff} = 3/2 (top row: easy axis as green dashed line; bottom row: hard axes as red dashed lines) for **1** (left column) and **2** (right column). Hydrogen atoms are omitted for clarity.

Table S10 Relative SO-RASSI energies and their Cartesian components of the *g*-tensor for S_{eff} = ½ for the lowest Kramers doublets (KDs) of the $^4A_2[^4F]$ ground state of the complexes **1**, **2**, **2** (κ = 170°), and **2** (κ = 160°)

		1	**2**	**2** (κ = 170°)	**2** (κ = 160°)
KD1	E_{KD1} / cm^{-1}	0	0	0	0
	g_x	0.172	0.133	0.073	0.232
	g_y	0.181	0.134	0.075	0.241
	g_z	7.673	7.682	7.653	7.818
KD2	E_{KD2} / cm^{-1}	64	66	64	74
	g_x	4.465	4.400	4.345	4.482
	g_y	4.143	4.177	4.233	4.082
	g_z	2.613	2.616	2.604	2.676

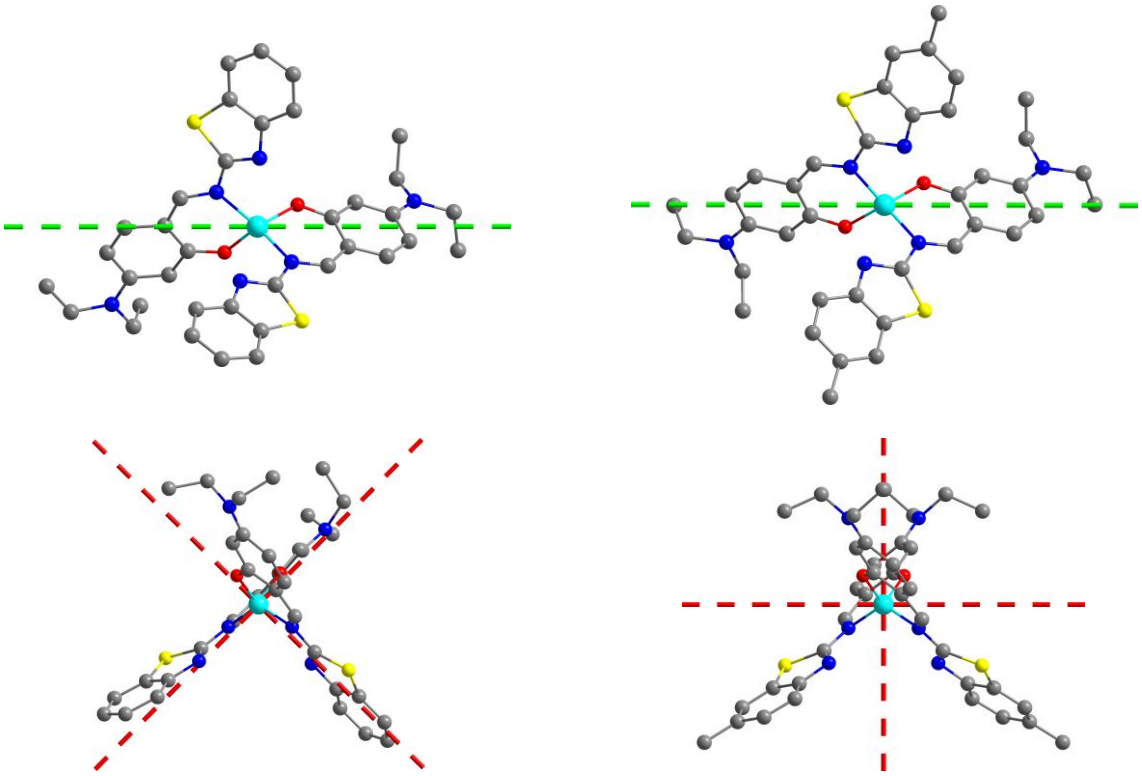

Fig. S16 *Ab initio* calculated magnetic axes for the ground state KD of **1** (left column) and **2** (right column) (top row: easy-axis of magnetization (green dashed line); bottom row: hard axes of magnetization (red dashed lines)). Hydrogen atoms are omitted for clarity.

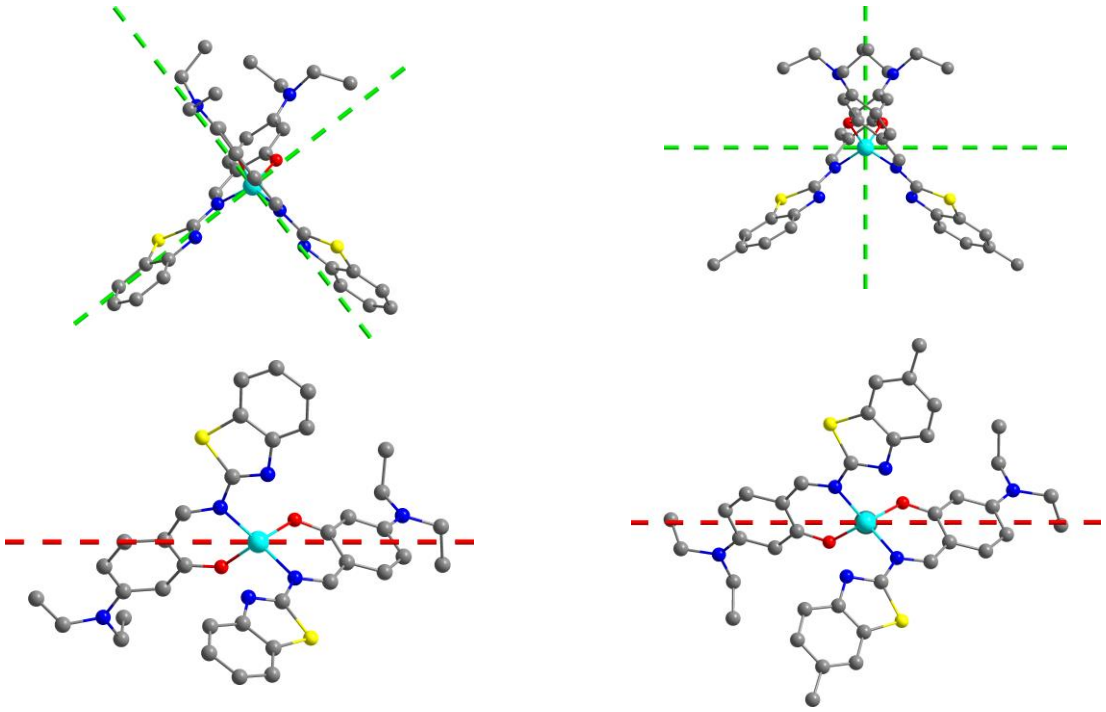

Fig. S17 *Ab initio* calculated magnetic axes for the first excited KD of **1** (left column) and **2** (right column) (top row: easy axes of magnetization (green dashed lines); bottom row: hard axis of magnetization (red dashed line)). Hydrogen atoms are omitted for clarity.